International Research Journal of Engineering and Technology (IRJET) e-ISSN: 2395 -0056
Volume: 02 Issue: 08 | Nov-2015 www.irjet.net p-ISSN: 2395-0072

Imaging through Kolmogorov model of atmospheric turbulence for shearing interferometer wavefront sensor

M.Mohamed Ismail [1] M.Mohamed Sathik [2]

[1]Research Scholar, Department of Computer Science, Sadakathullah Appa College, Tirunelveli, Tamilnadu, India.
[2]Principal, Sadakathullah Appa College, Tirunelveli, Tamilnadu, India.

Abstract - ***When observed with a ground based telescope, the image of a star is not sharp due to atmospheric turbulence. To overcome atmospheric turbulence for ground based telescope, astronomers have developed the technique of adaptive optics (AO) to actively sense and correct wave front distortions at the telescope during observations. A telescope with AO measures the wavefront distortions with a wavefront sensor and then applies phase corrections with a deformable mirror on a time scale comparable to the temporal variations of the atmosphere's index of refraction. Adaptive optics improves image resolution and increases the image's coherence. The main part of the AO system is to detect the incoming distorted wavefront. For this wavefront sensor based on polarization shearing interferometry technique has been studied. The necessary theory for shearing interferometry has been developed. Theoretical Simulations of the interferometric records were carried out for the study of various aberrations in an optical system and the effect of noise and atmospheric turbulence in the interferogram. In this paper, the physical background of imaging through turbulence, using Kolmogorov statistics with the Polarization Shearing Interferometry techniques have been discussed.***

Key Words: *Adaptive Optics, Shearing Interferometer, Kolmogorov model, atmospheric turbulence.*

1. INTRODUCTION

Ground based telescopes, the earth's atmosphere is always limiting factor for diffracted limited resolution [1]. This is because the atmosphere through which light from the stars propagate is turbulent and distort the wavefront [2]. The resolving power of a telescope when imaging through earth's atmosphere is not proportional to telescope diameter but to the characteristic coherence length of turbulence called Fried parameter r_0 [3]. The fundamental components of an adaptive optical (AO) system are a wavefront sensor to measure the distortions in the optical beam, a wavefront corrector to compensate these errors, and an estimation and control algorithm to derive the control signals from the distortion measurements. Fig.1 illustrates the schematic of an adaptive optics system.

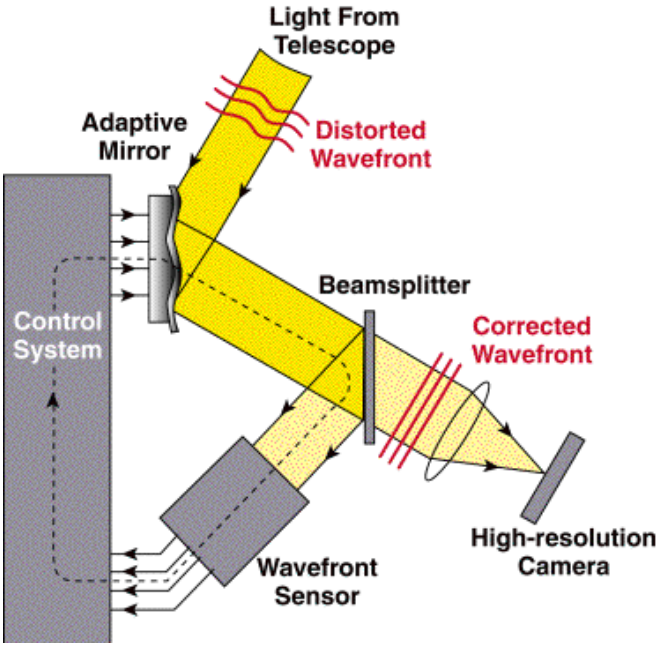

Fig-1. Schematic diagram of an Adaptive Optics System

Shearing interferometry has the important advantages over other wavefront sensors, it is very high resolution, the interferogram analysis is a global deformation analysis in the Fourier domain and that it requires no reference wavefront for the production of fringes other than the incident wavefront itself i.e. Self-referenced measurement and particularly insensitive to environment vibrations. In recently some methods based on Lateral shearing interferometry were employed as the wavefront sensor for real time atmospheric corrections [4, 5]. One of the major drawbacks of these interferometric techniques is the requirement of orthogonal pair of interferograms for wavefront reconstruction but shearing interferometer offers better choice for its linearity, better signal

processing and added spatial information. To study PSI, a simulation of wavefront has been generated and incorporated the wavefront errors caused due to atmospheric turbulence with varying noise levels and atmospheric turbulence. The theoretical simulation helps one to understand the behavior of the fringe patterns in different circumstances.

2. INTERFEROGRAM SIMULATION

It is important to understand the Polarization Shearing Interferometer theoretically and to sense the wavefront errors. A theoretical study has been undertaken. First, explanations about the simulations that were carried out with specific case of wavefront errors of an optical system [6] with respect to the Polarization Shearing Interferometer wavefront sensor are described. Secondly, the wavefront was generated using Zernike polynomials [7] and the wavefront errors caused due to atmospheric turbulence was incorporated. The errors due to the fabrication in terms of ripple and the noise were also simulated and presented. The theoretical simulation helps one to understand the behavior of the fringe patterns in different circumstances. Simulations were also carried out with varying noise levels and atmospheric turbulence. Simulations were carried using LABVIEW.

2.1 Mathematical Concepts

A simple wavefront equation having third order aberrations is derived from [8].

$$W(x,y) = A(x^2+y^2)^2 + By(x^2+y^2) + C(x^2+3y^2) + D(x^2+y^2) + Ey + Fx \quad (2.1)$$

Where A - Primary Spherical aberration, B -Primary Coma, C -Primary Astigmatism, D – Defocus, E - Tilt in X direction and F - Tilt in Y direction. When the shear value in X and Y directions are small, the shearing wavefront can be approximated as the first order derivative function as

$$\Delta W = \frac{\partial W}{\partial x}s + \frac{\partial W}{\partial y}t \quad (2.2)$$

where s and t are the shears in the x and y directions respectively. The intensity at the detector plane can be written as

$$I = K_0 + K_1 \cos\left(\frac{2\pi}{\lambda}\Delta W(x,y)\right) \quad (2.3)$$

2.1.1 Fringe Profiles in ideal conditions

In the case of Polarization Shearing Interferogram, the ideal conditions are described as the system having no aberrations but only defocus term. In order to study the effect of different aberrations, interferometric fringe profiles were simulated using the third order equations. Considering the equation 2.1 for the general wavefront, the sheared wavefront for various aberrations can be derived by Keeping only the defocus and taking the other coefficients A, B, C, E & F equal to zero, s and t are the shears in the x and y directions respectively. Fig.2 shows that the fringe profile in ideal condition (no aberration), and it was generated only by the defocus term which is given in eqn.2.5. These expressions are very similar to the one described by Malacara [6], except that these expressions are derived for two dimensional case.

$$\frac{\partial W(x,y)}{\partial x}s = 2D_1 xs, \frac{\partial W(x,y)}{\partial y}t = 2D_2 yt \quad (2.4)$$

and

$$D_1 = \frac{d_1}{2R_0^2} \text{ and } D_2 = \frac{d_2}{2R_0^2} \quad (2.5)$$

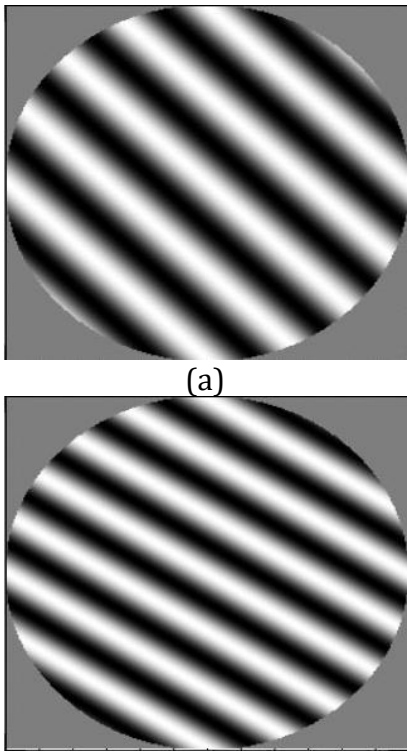

(a)

(b)

Fig- 2. Typical Polarization Shearing Interferogram in the presence of defocus only. (a). D1 = D2; (b) D1 ≠ D2;

2.1.2 Spherical aberration and Defocus

In the presence of spherical aberration the wavefront error takes the form as

$$\frac{\partial W(x,y)}{\partial x}s = 4Axs(x^2+y^2) + 2D_1xs \qquad (2.6)$$

$$\frac{\partial W(x,y)}{\partial y}t = 4Ayt(x^2+y^2) + 2D_2yt \qquad (2.7)$$

And the intensity at the detector plane is

$$I = K_0 + K_1\cos\left(\frac{2\pi}{\lambda}\{4Axs(x^2+y^2) + 2D_1xs\} + \{4Ayt(x^2+y^2) + 2D_2yt\}\right) \qquad (2.8)$$

Fig.3 Primary Spherical aberration and it was generated using only by the defocus & spherical aberration term and making all other values zero.

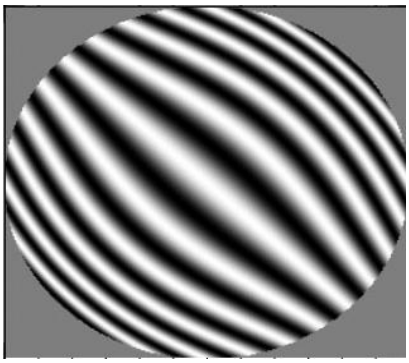

Fig -3.Primary Spherical aberration and Defocus

2.1.3 Primary Coma and defocus

In the presence of primary coma alone the wavefront error takes the form as

$$\frac{\partial W(x,y)}{\partial x}s = 2Bxys + 2D_1xs \qquad (2.9)$$

$$\frac{\partial W(x,y)}{\partial y}t = B(x^2+3y^2) + 2D_2yt \qquad (2.10)$$

And the intensity at the detector plane is

$$I = K_0 + K_1\cos\left(\frac{2\pi}{\lambda}\{2Bxys + 2D_1xs\} + \{B(x^2+3y^2) + 2D_2yt\}\right) \qquad (2.11)$$

Fig.4 Primary Spherical aberration and it was generated using only by the defocus & primary coma term and making all other values zero.

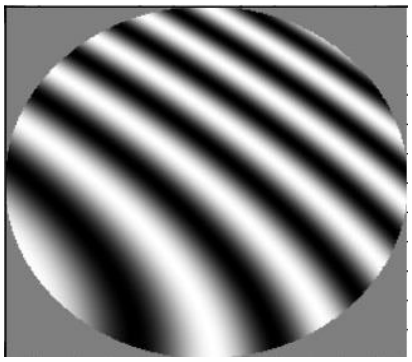

Fig- 4. Primary Coma and Defocus

2.1.4 Primary Astigmatism and defocus

In the presence of primary coma alone the wavefront error takes the form as

$$\frac{\partial W(x,y)}{\partial x}s = 2Cxs + 2D_1xs \qquad (2.12)$$

$$\frac{\partial W(x,y)}{\partial y}t = 2D_2yt - 2Cyt \qquad (2.13)$$

And the intensity at the detector plane is

$$I = K_0 + K_1\cos\left(\frac{2\pi}{\lambda}\{2Cxs + 2D_1xs\} + \{2D_2yt - 2Cyt\}\right) \qquad (2.14)$$

Fig.5 Primary Spherical aberration and it was generated using only by the defocus & primary astigmatism term and making all other values zero. Fig.6 presents with all errors present in the system except X & Y tilts.

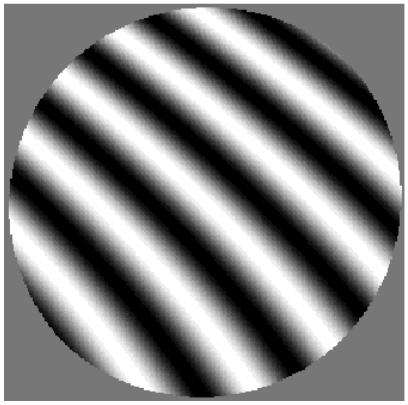

Fig.5. Primary Astigmatism and Defocus

2.1.5 All Primary Aberrations

When the wavefront error is assumed to have all the primary aberrations (Fig.6) then the intensity at the detector plane takes the form as

$$I = K_0 + K_1 \cos\left(\begin{matrix}\frac{2\pi}{\lambda}\{4Ax(x^2+y^2)+2Bxy+2Cxs+2D_1x+E\}s+ \\ \frac{2\pi}{\lambda}\{4Ay(x^2+y^2)+B(x^2+3y^2)-2Cy+2D_2x+F\}t\end{matrix}\right) \quad (2.15)$$

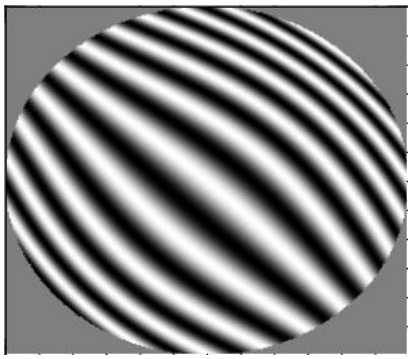

Fig - 6.All errors except X-Tilt and Y-Tilt

3. Interferogram Simulations using Zernike Polynomial

Zernike polynomials are widely used for describing the classical aberrations of an optical system [9]. They have the advantage that the low order polynomials are related to the classical aberrations like, spherical aberration, coma and astigmatism. Fried [10] used these Zernike polynomials to describe the statistical strength of aberrations produced by the atmospheric turbulence. The PSI wavefront sensor measures the wavefront slope. The derivatives of the Zernike Polynomials can be written as a linear combination of Zernike polynomial [7]. Hence, the slope information from the wavefront sensor can be conveniently expressed as a function of the Zernike polynomials. The basic interferometric equation for Zernike and the gradient of the Zernike polynomial is represented by

$$\Delta Z_j = \sum_{j'} \gamma_{jj'} Z_{j'} \quad (3.1)$$

where γjj are the coefficients of the Zernike expansion of the derivative of the jth Zernike. The matrix γ is called Zernike derivative matrix and it is given in Noll, 1976. And the wavefront slope is explicitly written as

$$\Delta W(x,y) = \sum_{j=1}^{n} a_j \left(s \sum_j \gamma_{x_{jj}} Z_j + t \sum_j \gamma_{y_{jj}} Z_j\right) \quad (3.2)$$

Where $\gamma_{jj'}$ is called Zernike Derivative matrix. Fig.7. shows that the simulation of interferogram using 11 Zernike coefficients which is given in [7].

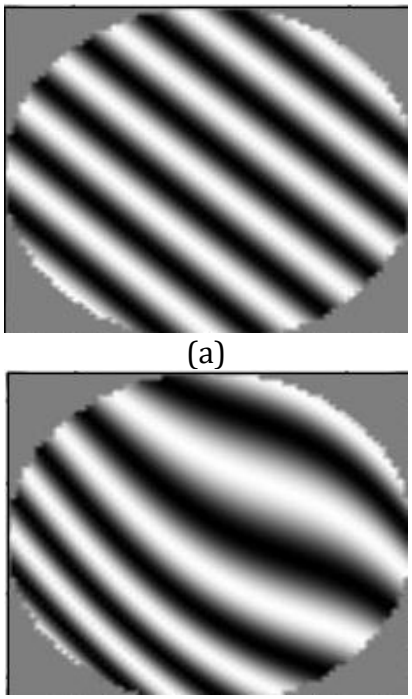

(a)

(b)

Fig.7. Simulated PSI interferograms using the Zernike coefficients (a) only defocus term and all other coefficients is zero. (b) inclusive of all(11) Zernike coefficients.

3.1 Effect of noise

The signal to noise ratio of an interferogram is a quality estimation factor. It is a measure of how strong the signal is with respect to the external noise present at the time of observation. The presence of random noise, alters the visibility and the contrast of the fringes drastically. For visualization and for illustration purposes, a random noise was additionally introduced in the same simulation. The effect of noise on PSI is shown in Fig.8.a. The next source of error comes from the inherent fabrication errors. These errors are from low frequency to high frequency components. The following Fig.8.b show the presence of ripples produced during the fabrication of the optics, which reduces the fringe visibility and introduces high frequency components into the system.

The ripples are the static errors which do not change in time. These errors can be evaluated and subtracted from the interferogram. Since these ripples and noise are of high frequency compared to the modulation frequency, it is convenient to remove these using Fourier transform technique. The effect of noise introduced in the interferometric equation as an added random term in the phase. The ripples are created as cosine function introduced into the phase factor of the interferometric equation.

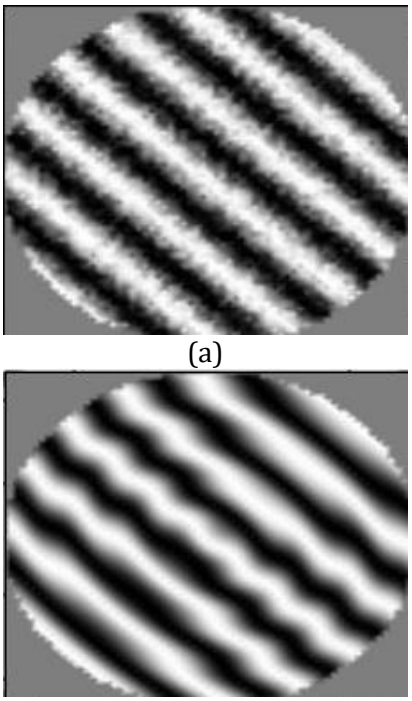

(a)

(b)

Fig.8. (a) A Noisy fringe pattern; (b) Ripple fringe pattern.

4. TURBULENCE MODEL GENERATION

The most widely accepted theory of turbulence flow, due to consistent agreement with observation, was by Andrei Kolmogorov [11]. Kolmogorov model assumes that energy injected into turbulent medium on large spatial scales (outer scale, L0) and forms eddies. These large eddies cascade the energy into small scale eddies until it become small enough (small scale, l0) that the energy is dissipated by the viscous properties of the medium. A statistical model of the wavefront aberrations induced by the turbulent atmosphere was proposed by Kolmogorov [12]. This model is based on the idea that energy is fed into the system at large scales and propagates down to smaller structures, where it eventually dissipates into heat. To describe the statistics of the wavefront aberrations, the power-spectral density (PSD) Ψ(κ) is defined. This is a measure of the relative contribution of aberrations with spatial frequency κ to the total wavefront distortion. For the Kolmogorov model, it is given by [7]

$$\Psi(\kappa) = 0.033 C_N^2 \kappa^{-11/3} \quad (4.1)$$

The scaling to different atmospheric conditions is accomplished with the refractive index structure function C_N^2. However, the Kolmogorov model is only useful between the largest (the outer scale L_0), and the smallest structures (the inner scale l_0) of the turbulence. At the ground, l0 is typically less than 10mm whereas L0 is of the order of a few tens of meters. The outer scale L0 limits the contribution of low spatial frequencies to the wavefront aberrations. Since these spatial frequencies dominate the overall wavefront distortions, L_0 has a significant influence on the achievable performance and image quality of future giant telescope or ground-based interferometers. Modified model of von Karman model power spectral density Φ_N of turbulence signal agrees well with the theory and experimental measurement, which is given by equation 4.2.

$$\Phi_N(K) = 0.033 C_N^2 (K^2 + K_0^2)^{-11/6} exp\left(-k^2/k_i^2\right) \quad (4.2)$$

Where $K_0 = 2\pi/L_0$, $K_i = 5.92/l_0$, and $K_0 = 2\pi/L$.

It can be expressed in another form with Fried parameter r_0. This power spectrum is only valid within the inertial range between the inner and outer scale as it tends to infinity at larger spatial separations. So in order to accommodate the finite inner and outer scales, the Kolmogorov power spectrum was modified by Von Karman power spectrum which is given by.

$$\Phi_N(K) = 0.023 (D/r_0)^{5/3} \frac{\exp(-k^2/k_i^2)}{(k^2/k_0^2)^{11/6}} \quad (4.3)$$

Fried parameter which measures the optical quality of atmosphere expressed as given below as a function of refractive index profile $C_n^2(Z)$ and zenith angle ζ. Where $C_n^2(Z)$ is the structure constant for the refractive index of atmosphere with altitude z, measured in $m^{-2/3}$.

$$r_0 = [0.423 K^2 sec\xi \int C_n^2(Z) dz]^{-3/5} \quad (4.4)$$

The Eqn. 4.4 can be rewritten in another form as the function of Fried parameter r_0,

$$\emptyset_N(K) = 0.023\left(\frac{D}{r_0}\right)^{5/3} \frac{\exp\left(-\frac{K^2}{K_i^2}\right)}{\left(K^2+K_0^2\right)^{\frac{11}{6}}} \qquad (4.5)$$

In the following, the physical background of imaging through turbulence, using Kolmogorov statistics, and the Polarization Shearing Interferometry techniques to sense and to correct the wavefront aberrations with adaptive optics have been discussed. Based on the Eq. (4.5) numerical simulations of atmospheric turbulence called phase screen has been carried out by using Fourier transform and Sub harmonics methods explained below.

4.1 Fourier transforms method

Fourier transform method proposed by McGlamery [13, 14] has been used to simulate the phase screens numerically and considered only phase distribution as the phase variations across the wavefront are the dominant image degrading component. One way of describing the phase statistically is by means of its power spectrum. The method of generating an instantaneous phase map using the power spectrum is based on the assumptions of

1) The modulus of the Fourier transform of the phase map is a random variable. At any given frequency the modulus is a Rayleigh random variable with zero mean over an ensemble average and with a variance, over an ensemble average, equal to the value of the Kolmogorov power spectrum.

2) The phases of the Fourier transform of the phase map are independent with frequency, uniformly randomly distributed in the –π to + π interval. Based on these assumptions the phase map is generated using a complex array of Gaussian random numbers is generated and the array is multiplied by the square root of the power spectrum ($f^{-11/6}$). The array is subjected to a discrete Fourier transform and the resulting complex array is separated into its real and imaginary components, each of these arrays represent an independent instantaneous phase map realization.

The power spectral density of atmosphere Φ_N (κ) and phase screen signal p(r) are related as

$$\text{?}_N(K) = \left|\int_{-\infty}^{\infty}\int_{-\infty}^{\infty} p(r)\exp(-iKr)\,dr\right|^2 \qquad (4.6)$$

Phase screen p(r) can be obtained from above equation,

$$p(r) = \int_{-\infty}^{\infty}\int_{-\infty}^{\infty}\sqrt{\text{?}_N(K)}\exp(iKr)\,dk \qquad (4.7)$$

Where p(r), is a two dimensional Kolmogorov phase screen, which is obtained from inverse 2D Fourier transform of the square root of von Karman power spectrum of turbulent atmosphere. The randomness of atmospheric turbulence implemented with random numerical function. This method has a disadvantage of under sampling at low spatial frequencies due to limited low sampling of Fourier transform technique. The Fig. 9(a) presents the typical atmospheric phase screen simulated by fourier transform method with D/ro= 5, L0=50 m, l0=0.01 m. The Fig. 1(b) demonstrates 3D representation of phase screen. The Fig. 1 (c) Represents the interference fringe pattern with a turbulent phase screen of D/r0 =0.01 and Fig. 1 (d) shows after rotating the image by 450 of fig.9.(C). In this figure one can observe that the low spatial frequencies are not sampled well (i.e., no tip/tilt).

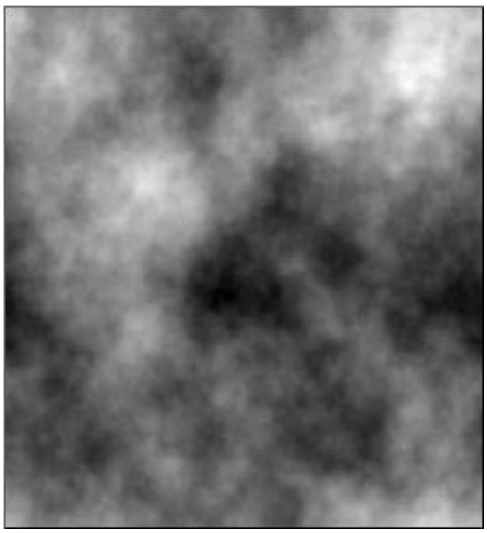

(a)

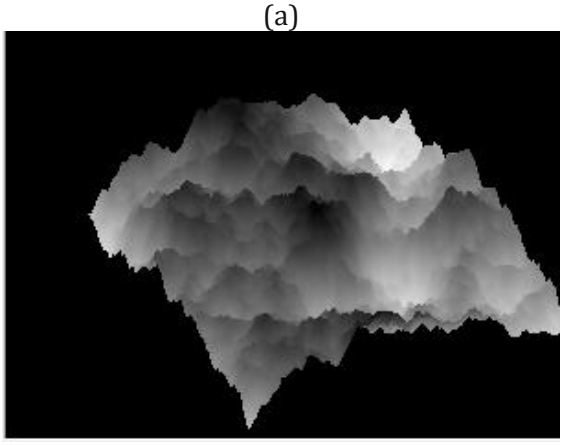

(b)

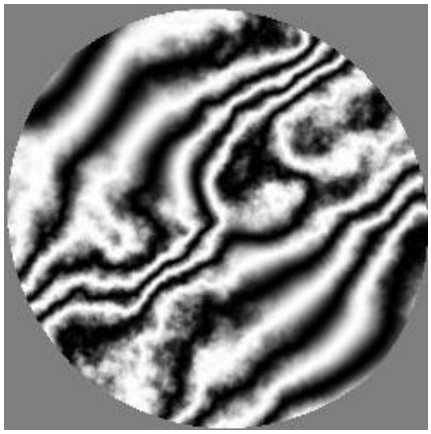

(c)

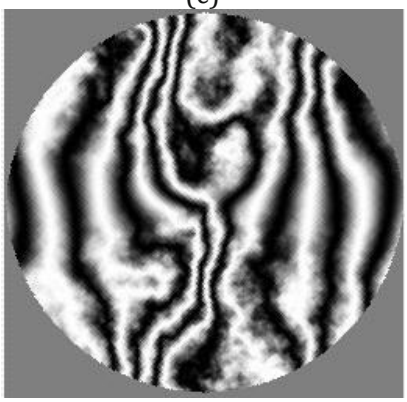

(d)

Fig- 9. Sample phase screens obtained by Fourier transform method (a & b) and representation of the interference fringe pattern with a turbulent phase screen (c &d)

4.2. Sub-harmonics method

Sub harmonics method [15, 16] is a simple technique for modeling the effects of lower frequencies to generate additional random frequencies and add their effects to the sampled frequencies given by Eq. (4.8). It modifies the usual FFT method of generating phase screens for atmospheric propagation to allow for low-frequency turbulence effects. The method consists of generating realizations of turbulence on two different size grids and using a trigonometric interpolation to introduce low-frequency effects on the smaller (propagation) grid. It is proved that the phase screens generated by this method give a better representation of Kolmogorov turbulence since they include effects from the low-spatial-frequency part of the spectrum. This method can be considerably more efficient than a straightforward implementation of the FFT method on a very large grid. It provides a low frequency screen p(x,y) is generated by sum of different number (Np) of phase screens, one can write low frequency screen as a Fourier series given by

$$p(x,y) = \sum_{g=1}^{N_g} \sum_{n=-1}^{1} \sum_{m=-1}^{1} c_{n,m} \exp\left[i2\pi\left(f_{xn}\,x + f_{ym}\,y\right)\right] \quad (4.8)$$

Where, the sums over n and m are over discrete frequencies and each value of the index g corresponds to a different grid. The final phase screen generated in this simulation is derived by addition of two phase screens obtained with Fourier transform method and sub harmonics method. The sample phase screens thus simulated are shown in Fig. 10. The Fig. 10(a) presents the typical atmospheric phase screen simulated by sub harmonics method with D/r_0= 5, L0=50 m, l0=0.01 m. The Fig. 10(b) demonstrates 3D representation of phase screen. The Fig. 10 (c) Represents the interference fringe pattern with a turbulent phase screen of D/r0 =0.01 before rotation and Fig. 10 (d) shows after rotating the image by 450 of fig.10.(C). In this figure it is clearly seen that low spatial frequencies are well sampled.

(a)

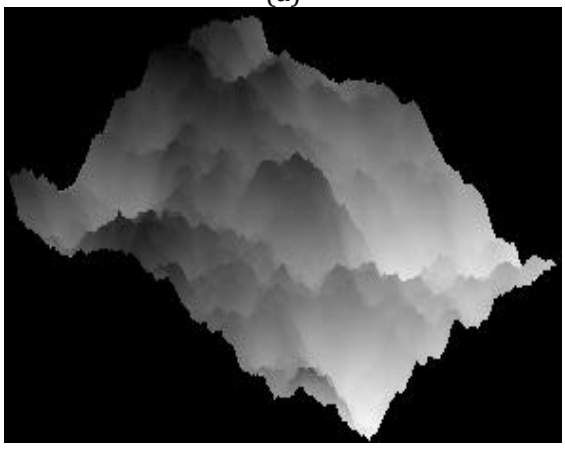

(b)

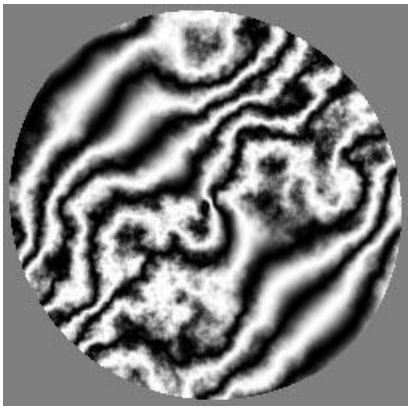

(c)

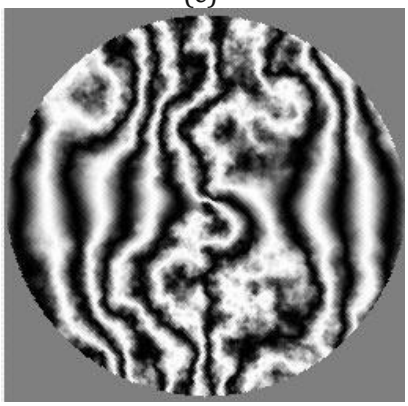

(d)

Fig - 10. Sample phase screens obtained by sub harmonics method (a & b) and representation of the interference fringe pattern with a turbulent phase screen (c & d)

5. CONCLUSION

In this paper, we attempted to simulate the fringe pattern with respect to shearing interferometer for specific case of wavefront errors of an optical system and wavefront was generated using Zernike polynomials. The wavefront errors caused by atmospheric turbulence were incorporated by simulating numerically which follows the von Karman turbulence model. The turbulence model was simulated using FFT method and Sub harmonics method and fringes affected by both this methods was integrated.

REFERENCES

[1] S.K. Saha, Diffraction limitted imaging with large and moderate telescopes (World Scientific, Singapore, 2007)

[2] M.C. Roggemann, B.M. Welsh, Imaging through turbulence, (CRC Press, Laser & Optical Science & Technology Series, 1996)

[3] D.L. Fried, Anisoplanatism in adaptive optics. J Opt Soc Am 72, 52–52 (1982)

[4] J.W.Hardy, J.E.Lefebvre and C.L.Koliopoulous, "Realtime atmospheric compensation." J.Opt.Soc.Am. 67, 360-369 (1977).

[5] J.W.Hardy, "Adaptive Optics: a new technology for the control of light," Proc.IEEE 66, 651-697 (1978).

[6] Malacara, D. Optical Shop Testing, 2nd Edn. John Wiley & Sons, (1992).

[7] Noll, R.J., " Zernike polynomials and atmospheric turbulence" J. Opt. Soc. Am., Vol. 66, No.3, 207 – 211 (1976).

[8] Kingslake R, "Lens Design Fundamentals", Acad. Press (1978).

[9] Born E and Wolf, "Principles of Optics" Pergamon Press. (1970).

[10] Fried, D.L. "Statistics of a geometrical representation of wavefront distortion" J.Opt.Soc.Am., Vol.55, No.11, 1427 – 1435 (1965).

[11] A. N. Kolmogorov. The local structure of turbulence in incompressible viscous fluid for very large Reynolds numbers (translation). Proceedings of the Royal Society of London A, 434:9-13, 1991.

[12] V.I. Tatarski. Wave Propagation in a Turbulent Medium. McGraw-Hill, 1961.

[13] B.L. McGlamery, in Computer simulation studies of compensation of turbulence degraded images, ed. by J.C. Urbach. Image processing, Proc. Soc. Photo-Opt. Instrum. Eng. 74, 225–233 (1976)

[14] E.M. Johansson, D.T. Gavel, Simulation of stellar speckle imaging, ed. by J.B. Breckinridge. Amplitude and intensity spatial interferometry II, Proc. SPIE 2200, 372–383 (1994)

[15] B.J. Herman, L.A. Strugala, Method for inclusion of low frequency contributions in numerical representation of atmospheric turbulence, ed. by P.B. Ulrich, E. Wilson. Propagation of high-energy laser beams through the earth's atmosphere, Proc. SPIE 1221, 183–192 (1990)

[16] R.G. Lane, A. Glindermann, J.C. Dainty, Simulation of a Kolmogorov phase screen. Waves Random Media 2(3), 209–224 (1992

BIOGRAPHIES

Mr. M.Mohamed Ismail is Research Scholar at Sadakathullah Appa College, Tirunelveli. He obtained his M.Sc degree in Information Technology from Bharathidasan University and completed M.Tech degree in Information Technology from Karnataka University. He has been involved in the software development of various optical and astronomical instruments. His current interests are focused on developing software for shearing interferometer based wavefront sensing in Adaptive Optics.

Dr.M.Mohamed Sathik is working as Principal, Sadakathullah Appa College, Tirunelveli. He has completed M.Phil. Computer Science and Ph.D. Computer Science in Manonmaniam Sundaranar University, Tirunelveli. He has involved in various academic activities. He has more than 100 research publications in journals. He has attended many national and international seminars, conferences and presented numerous research papers. He has guided more than 30 research scholars and also published two books. He is a member of curriculum development committee in various universities and autonomous colleges of Tamilnadu and his area of specialization are Virtual Reality, Image Processing and Sensor Networks.